A multi-level investigation on the mechanical response of TRM-strengthened masonry

Dalalbashi, Ali; Ghiassi, Bahman; Oliveira, Daniel V.

DOI:
10.1617/s11527-021-01817-4

A multi-level investigation on the mechanical response of TRM-strengthened masonry

Ali Dalalbashi[1], Bahman Ghiassi[2], Daniel V. Oliveira[3]

ABSTRACT

This paper presents a multi-level experimental and analytical investigation on the mechanical performance of TRM composites used for strengthening existing masonry structures. Micro (fabric-to-mortar bond), meso (TRM-to-substrate bond), and macro (TRM tensile response and in-plane and the out-of-plane response of TRM-strengthened masonry) response of TRMs are combined and investigated in-depth for this reason. These results help understand the mechanisms controlling the response of these composites and their performance at the structural scale.

Keywords: *TRM; FRCM; TRM-strengthened masonry; in-plane behavior; out-of-plane behavior, multi-level experimental testing.*

[1] PhD Student, ISISE, Department of Civil Engineering, University of Minho, Guimarães, Portugal. E-mail: alidalalbashi@gmail.com. https://orcid.org/0000-0003-0486-1433

[2] Assistant Professor, Centre for Structural Engineering and Information, Faculty of Engineering, University of Nottingham, Nottingham, United Kingdom. E-mail: bahman.ghiassi@nottingham.ac.uk. http://orcid.org/0000-0003-4212-8961

[3] Associate Professor, ISISE, Department of Civil Engineering, University of Minho, Guimarães, Portugal. E-mail: danvco@civil.uminho.pt. http://orcid.org/0000-0002-8547-3805

1 Introduction

Many unreinforced masonry (URM) structures are prone to catastrophic failure during earthquakes [1, 2] due to their weakness against in-plane and out-of-plane seismic loads [3]. The development of strategies for the repair and strengthening of structures made of these materials has been the object of many studies during the last decades. Among these, externally bonded reinforcement is one of the most common strengthening methodologies, in which composite material is attached to the external surface of weak structural components. Traditionally, Fiber Reinforced Polymers (FRPs) were mainly used as the strengthening material in this system. However, the issues related to sustainability, durability, poor performance at high temperature, and compatibility of these composites with masonry indicated the need to use and develop novel repair materials. In an attempt to alleviate the drawbacks that arise from the use of FRPs [4, 5], Textile Reinforced Mortar (TRM) composites have been proposed in the last years [6, 7].

TRMs are composed of continuous yarns/fibers embedded in an inorganic matrix and present several advantages: they have a high thermal capacity, are applicable to wet surfaces, are removable, and can be compatible with masonry and concrete surfaces [4, 8]. The large variety of available fabric types and mortars allows TRM composites to develop with an extensive range of mechanical properties [9, 10]. When properly designed, TRMs show a pseudo-ductile response with distributed cracking, which makes them interesting for seismic strengthening applications [11, 12].

Despite the recent attention these composites have found as a suitable strengthening material, many issues regarding the mechanical response and durability of these composites are still unknown. Recent studies have mainly focused on the tensile response of TRMs and the bond of TRM-to-masonry. Studies at the structural scale [13–15] or the composite scale [16–19] can also be found. However, comprehensive experimental/analytical studies from materials to structural scale are still missing [20, 21]. Structural scale tests (diagonal tension or out-of-plane tests on TRM-strengthened masonry) are still few and mainly focused on the effect of textile and substrate types [22, 23], the number of textile layers [24], and symmetrical or asymmetrical application of the repair [13, 25, 26]. Nevertheless, there is a lack of understanding of the parameters controlling the response at the structural scale. This understanding will be developed in this paper through a comprehensive experimental and analytical study from materials to structural scale.

2 Experimental program

The experimental campaign consisted of materials mechanical characterization tests, textile-to-mortar pull-out tests, TRM-to-substrate bond tests, TRM direct tensile tests, and finally, diagonal compression and flexural tests on TRM-strengthened masonry panels. The role of sandblasting of the masonry surface is also investigated. A detailed description of the materials, preparation of specimens, and the test methods are presented in this section and Online Resource 1. The timeline used for the samples' preparation and testing is presented in Fig. 1 to facilitate understanding the sequences and the considered framework.

2.1 Materials

Solid clay bricks (200×100×50 mm^3) were used to construct the masonry wallets and the single-lap shear specimens. Two different lime-based mortars were used in this study, referred to as M1 and M2. M1 mortar is a high-ductility hydraulic mortar and is commercialized as a TRM matrix (Planitop HDM Restauro). This two-component mortar was prepared by mixing the powder and liquid in a low-speed mechanical mixer to form a homogeneous paste. M2 mortar was utilized to build the masonry wallets and is also based on lime and ecopozzolan (Mape-Antique MC). The TRM composite used here is a glass-based TRM. The glass fabric was a woven biaxial fabric mesh made of alkali-resistance fiber glass (Mapegrid G220). Its mesh size and area per unit length are equal to 25×25 mm^2 and 35.27 mm^2/ m, respectively.

2.2 Material characterization tests

The compressive and flexural strength of the mortars was tested according to ASTM C109 [27] and EN 1015-11 [28]. Five cubes (50×50×50 mm^3) and five prismatic (40×40×160 mm^3) specimens were prepared for each mortar. The M1 mortar strength was measured after 28 and 90 days, while M2 mortar strength was tested after 28 and 120 days (see also Fig. 1). Elastic modulus and splitting tensile strength of the mortars were tested according to EN 12390-13 [29] and ASTM C496 [30]. Five cylinders with 70 mm diameter and 150 mm in length were made for each test, totaling ten specimens for each mortar type. In this part, samples were demolded after three days and placed in a damp environment for seven days; then, samples were cured in the lab environmental conditions (20°C, 67% RH) until testing.

The brick's compressive strength was characterized according to ASTM C67 [31] and EN 772-1 [32] and along with all directions, i.e., flatwise, lengthwise, and widthwise directions. For each

direction, five cubes (40×40×40 mm^3) were used. Flexural strength and elastic modulus of the brick were calculated according to EN 1015-11 [28] and EN 12390-13 [29], respectively, by using five prismatic specimens (40×40×160 mm^3) for each test. For measuring the flexural strength, the load was applied perpendicular to the flatwise and lengthwise surface of the brick; while, the elastic modulus was measured along the lengthwise direction only.

The compressive and the flexural tests were performed using a Lloyd testing machine under force-controlled conditions at a rate of 150 N/s and 10 N/s, respectively. In the compressive tests, a pair of Teflon sheets with a layer of oil between them was placed between the specimen and the compression plates for reducing the possible friction effect. For measuring the elastic modulus, a universal testing machine (load capacity of 100 kN) and LVDTs (3 for cylinder and 4 for prismatic specimens) with a 5 mm range and 1-µm sensibility were used. Tensile splitting tests were also performed using the universal testing machine and introducing monotonic displacements at a rate of 0.12 mm/min.

The compressive strength of masonry prisms was obtained according to ASTM C1414 [33] by conducting the tests on prisms made of three bricks and M2 bed joint mortar with about 20 mm thick. These tests were performed at 28 and 120 days (five specimens at each age). A universal testing machine with a load capacity of 1000 kN under displacement-controlled conditions (0.3 mm/min) was used to apply the load perpendicular to the flatwise direction of bricks. Additionally, the shear strength of five triple-brick prisms was investigated at 28 days age based on EN 1052-3 [34]. Before applying the shear load, the pre-compression load was applied to the specimens. A universal testing machine (load capacity of 100 kN) under displacement-controlled conditions (0.3 mm/min) was used to apply the load parallel to the bricks' lengthwise direction.

The tensile strength and elastic modulus of the fabrics in both warp and weft directions were measured through direct tensile tests on single yarn. A universal testing machine (load capacity of 10 kN) was used for this purpose. The tests were performed on five specimens with a free length of 300 mm under displacement-controlled conditions (0.3 mm/min). A 100 mm clip gauge, which was located at the center of the specimen, and the internal LVDT of the machine measure the yarn deformation.

2.3 Pull-out test

The single-sided pull-out test setup developed in [35] was used for studying the bond behavior between the yarn and the mortar. The specimens were prepared by embedding single yarns in a disk-shaped mortar with a cross-section of 125×16 mm^2 for 50 and 100 mm (Fig. 2a). Before this, the free end of the yarn was covered with an epoxy resin block with a rectangular cross-sectional area of 10×16 mm^2 and 200 mm long [35]. Specimens were demolded after three days of preparation and covered by wet clothes and plastic for seven days. Those were then placed in the lab environmental conditions (20°C, 67% RH) and tested after 90 days of age. Five samples were prepared and tested under the pull-out testing scheme in total.

The test setup consisted of U-shape steel supports attached to a rigid frame to fix the samples (Fig. 2a). The tests were performed using a servo-hydraulic system with a maximum capacity of 25 kN and a mechanical clamp that pull the epoxy resin from the top. In another study conducted by the authors [36], displacement rate effects on the pull-out response of glass-based TRM were investigated. The results illustrated that the bond behavior did not show any considerable changes by increasing the rate from 0.3 mm/min to 1.0 mm/min. Hence, to save time, the pull-out test's displacement rate in this study was adopted at 1.0 mm/min. Three LVDTs recorded the slip with a 20 mm range and 2-µm sensibility, as shown in Fig. 2a. The mean values of these LVDT measurements are presented as the slip in the experimental results.

2.4 TRM tensile test

Five prismatic (550×70×10 mm^3) specimens were prepared for performing direct tensile tests, as shown in Fig. 2b. The fabric mesh consisted of three warp and 13 weft glass yarns, in which the warp yarns were parallel to the tensile load direction. The samples included a 100 mm free yarn length at each side and a 350 mm central region in which the fabrics were embedded in the mortar (Fig. 2b). The curing conditions of these samples were similar to the pull-out test specimens.

One week before the tests, two steel plates (100× 75× 10 mm^3) were attached to the free part of yarns after saturating it with resin to avoid rupture of the clamping fabric area during the tests. Two mechanical clamps gripped the samples, and two LVDTs with a 20 mm range and 2-µm sensibility were placed at both sides of the tensile specimen to record the deformation, as illustrated in Fig. 2b. A servo-hydraulic jack with a maximum capacity of 25 kN applied the direct tensile load to the specimens through the clamps under a displacement control rate of 0.3 mm/min. The

results are presented in terms of stress-strain curves in section 3.3. The stress introduced to the samples was calculated considering the cross-section area of the yarn. Simultaneously, the strain was computed by dividing the mean value of the displacements recorded from the two LVDTs by their base length (310 mm).

2.5 Single-lap shear test

Single-lap shear specimens were prepared by applying the TRM composite to the bricks flatwise surfaces. Two groups of samples were prepared with 100 mm bonded length. In one group, the original brick surface was used (method a), while in the second group, the brick surface was sandblasted to increase the surface roughness, here termed method b [37]. Besides, to investigate the effect of bond length, an additional embedded length of 150 mm was utilized with sandblasted bricks (method b). Before applying the TRM composite, the bricks were pre-wetted for one hour to ensure a semi-saturated condition. The width and the total thickness of TRM were equal to 70 mm and 10 mm, respectively, as shown in Fig. 2c. The embedded glass mesh included three warp yarns, three transverse elements for 100 mm, and five transverse elements for 150 mm bond length, while the free length of the fabrics was 250 mm. For each type of brick surface and embedded length, five specimens were constructed and named as SL100-a for the original brick and SL100-b and SL150-b for single-lap shear specimens constructed with the sandblasted brick. The curing condition of these samples was similar to the pull-out test specimens.

For performing the tests, two aluminum plates ($65\times65\times2$ mm^3) were glued to the extremity of the yarns after saturating yarns with resin seven days before testing to facilitate the gripping and ensure a uniform load transfer. A stiff supporting frame and two clamps supported the specimens, as shown in Fig. 2c. Two LVDTs with a 20 mm range and 2-µm sensibility were placed at the loaded end to measure the slip during the tests. A servo-hydraulic jack with a maximum load capacity of 50 kN was used to perform the single-lap shear tests at a displacement rate of 0.3 mm/min. A preload equal to 100 N was applied to specimens before testing to facilitate the LVDTs attachment [38].

2.6 Masonry wallets

Solid clay brick and M2 mortar were used to build the masonry wallets. Again, to investigate the brick surface preparation effect on the structural performance of TRM-strengthened masonry, two groups of samples were prepared: in one group, original bricks were used, while in the second

group, sandblasted bricks were used (lengthwise direction) to build the wallets. Similar to single-lap shear specimens, bricks were immersed in water for one hour before being used. Thirty days after constructing and curing wallets in lab environmental conditions (20°C, 67% RH), TRM composites were applied (with 10 mm thickness mortar), and wallets were stored in the lab 90 days. Hence, wallets were tested after 120 days. The wallets strengthened with TRM composites were cured under wet clothes and plastic during the first week, similar to the procedure considered for the pull-out and single-lap shear tests.

2.6.1 Diagonal compression tests

According to ASTM E519 [39], diagonal compression tests were performed on masonry wallets with dimensions of 540×540×100 mm^3, as shown in Fig. 3a. Nine wallets were constructed so that three of them were unreinforced masonry panels (named IU), while six others were strengthened by one layer of glass-based TRM composite applied on both faces. Three out of the six strengthened panels were made with the original bricks (named ISa), and the other three with the sandblasted bricks (named ISb). A servo-hydraulic system with a maximum capacity of 300 kN was used for performing these tests at a displacement rate of 0.3 mm/min. The load was applied through steel shoes (115×115×15 mm^3) placed at diagonally opposing bottom and top corners of the wallets [15]. As shown in Fig. 3a, two 20 mm range and 2-μm sensibility LVDTs measure the vertical and horizontal deformation of the wallets during the tests.

2.6.2 Out-of-plane tests

Flexural tests were performed promoting preferential damage and failure either parallel or normal (perpendicular) to bed joints and according to EN 1052-2 [40]. Nine specimens were prepared for each direction. Therefore, three wallets were un-strengthened, and six (3 sandblasted and 3 original) were strengthened with TRM only at one side of the wallets (opposite side of the loading). Dimensions of the out-of-plane wallets failure parallel and normal to bed joint were 540×420×100 mm^3 and 520×330×100 mm^3, respectively, as shown in Fig. 3b and Fig. 3c. Based on EN 1052-2 [40], for wallets failure parallel to bed joint, minimum two bed joints should be within the inner support (constant moment length), see Fig. 3b. However, for wallets failure normal to bed joint minimum one head joint must be within the inner support (Fig. 3c). The fabric mesh was placed so that the warp yarns were parallel to the longitudinal axis of specimens. In total, there were 17 and 12 warp yarns in the out-of-plane wallets parallel and normal, respectively. Meanwhile, 21 weft yarns were in both types of flexural wallets.

Specimens were tested in a vertical configuration (to omit the effect of specimens' self-weight on the results) under four-point bending so that the strengthened face was subjected to tension. The distance between the outer and inner bearings was 420 mm and 170 mm, respectively. Four LVDTs were used with a 20 mm range and 2-μm sensibility to measure the sample deformation at the middle and the location of inner bearings, as shown in Fig. 3b and Fig. 3c. The tests were performed at a displacement rate of 0.3 mm/min and with a servo-hydraulic jack with a maximum load capacity of 50 kN.

These specimens are named XYZ, in which X is related to the type of out-of-plane failure (P or N), Y represents the existence of un-reinforced (U) or strengthened (S), and Z is linked to the brick surface "a" for original brick, and "b" for sandblasted brick. For example, wallet NSa is an out-of-plane wallet failure normal to the bed joints, strengthened and constructed by the sandblasted bricks.

3 Results and discussion

3.1 Material characterization results

Table 1 presents the mean strengths of the mortars and the brick. It can be observed that by increasing the mortar age, the compressive strength of both M1 and M2 mortars increases by 40% and 64%, respectively, from 28 to 90 days. A similar increase is observed for the splitting tensile strength (56% and 67%, respectively for M1 and M2 mortar), while the flexural and elastic modulus do not show any considerable change. This observation recalls that the maximum strength of the utilized lime-based mortars does not reach its peak value after 28 days, as opposed to cementitious mortars [41]. In another study conducted by authors [36], the compressive strength of M1 mortar, which was cured only one day under plastic and then stored in the environmental lab (20°C and 60% RH), reached 7.07 MPa and 7.84 MPa for 28 and 90 days, respectively. These values are 12.0 MPa and 16.8 MPa in this work, being 1.7 and 2.1 times that of the previous study. This difference is due to more appropriate curing conditions considered in this study (covered by wet clothes and plastic for seven days and then stored in a 20°C and 67% RH environmental lab). The brick compressive strength is different in each direction owing to its anisotropic properties, as reported in Table 1. Meanwhile, the flexural strength of the clay brick is almost equal in flatwise and lengthwise directions. Additionally, the mean compressive strength of the masonry prism after 28 days is equal to 10.9 MPa with a coefficient of variation (CoV) of 8 %. This value for the 120

days age is 11.1 MPa (CoV=8 %). Although the compressive strength of M2 mortar increases considerably, it does not significantly affect the compressive strength of the prism. The shear strength of masonry prisms at 28 days is equal to 0.26 MPa (CoV=18 %).

The average tensile strength, Young's modulus, and rupture strain of the warp glass yarn are 875 MPa (CoV=13 %), 65.94 GPa (CoV=5 %), and 1.77 % (CoV=10 %), respectively. These values for the weft direction are 685 MPa (9 %), 69.87 GPa (4 %), and 1.45 % (11 %), respectively. This observation shows that the tensile strength of the weft glass yarn is less than the warp yarn by 78%, and one should consider when analyzing the behavior of TRM-strength masonry panels.

3.2 Pull-out response

Fig. 4 shows the load-slip curves of the single glass yarn-based TRM for 50 and 100 mm bond length. As shown in Fig. 4, the load-slip curves of the specimens with 50 mm and 100 mm embedded length are different, which is due to the differences in their failure modes. For 100 mm embedded length, yarn rupture occurs after reaching the full strength of the yarns (as shown in Fig. 4b). This observation shows that a 100 mm embedded length is longer than the effective bond length, which is in line with [42]. The mean values of the main characteristics of the pull-out response are summarized in Table 2, which are the peak load (P_P) and its corresponding slip (S), debonding and pull-out energy ($E_{deb.}$, $E_{pull.}$), and initial stiffness according to [42]. Additionally, the bond-slip law parameters for 50 mm embedded length are presented in Table 2, including pull-out bond shear strength (τ_{max}), frictional shear strength (τ_f), bond modulus (κ), and slip-hardening coefficient (β). For calculating these parameters, the reader is referred to [35]. In the next sections, τ_f will be used to predict the crack spacing in tensile tests. For the purpose of determining bond parameters, the slip at the yarn-to-mortar interface is considered a fundamental property [35]. For 100 mm embedded length, because slippage between the yarn and the mortar is either nonexistent or very low, bond parameters could not be extracted for these samples.

3.3 TRM tensile behavior

The tensile response of the tested composites is shown in Fig. 5. All the samples failed by rupture of the yarns implying the adequacy of the clamping system used. The crack patterns developed in the samples are also shown in Fig. 5. On average, three cracks with an average distance of 101 mm are formed on the samples (Table 2). This crack spacing indicates that the pull-out test results

obtained from samples with 50 mm embedded length need to be used to interpret the bond effects on the post cracking response of these composites.

The main characteristics average value of the tensile response of specimens are also obtained and presented in Table 2 in terms of elastic modulus (E_1, E_2, E_3), strain (ε_1, ε_2, ε_3), and stress (σ_1, σ_2, σ_3) corresponding to linear stage, crack development stage, and post-cracking stage [41]. The mean value of the maximum tensile stress is equal to 995.6 MPa that is slightly higher than the tensile strength of the single yarns. This observation shows the stress has been distributed uniformly among the yarns, and the composite action has also slightly enhanced the final tensile response of the TRM system.

Comparing these results with the ones previously presented by the authors in [41] (where a different curing regime was followed: i.e., the specimens were cured for one day under plastic and then stored in the environmental lab for 90 days and therefore) shows the importance of curing conditions on the mechanical response of these composites (the results presents in this paper are around 1.6 times higher for the cracking strength and 5.6 times for the elastic modulus). Meanwhile, the saturated cracking distance is 1.58 times larger in the present study due to higher bond strength in samples cured under better conditions.

3.4 TRM-to-substrate bond behavior

A comparison among the results of SL100-a, SL100-b, and SL150-b specimens clearly shows the effect of sandblasting on the TRM-to-substrate bond behavior, see Fig. 6. The failure mode of the SL100-a samples is the delamination of the TRM from the substrate, while yarns slippage, followed by tensile rupture, is observed in the SL100-b samples. Additionally, in SL150-b specimens, all yarns ruptured by reaching the maximum load. The load-slip curves are also consequently different in these three sets of samples.

The main experimental parameters, such as the peak load (P_P) and its corresponding slip (s), the fabric stress (σ), and the initial stiffness (K) are obtained for the tested samples and presented in Table 2. σ is calculated by dividing the peak load by the cross-section area of the yarns (2.65 mm^2). It can be seen that sandblasting has a significant effect as SL100-b samples show a peak load and a corresponding slip around 2.14 times higher than those of SL100-a. Also, the initial stiffness of SL100-b specimens is 2.12 times higher than the SL100-a samples. As expected, by increasing the embedded length, the peak load and its corresponding slip increase by 44% and 33% in SL150-b

specimens compared to SL100-b specimens. The initial stiffness of SL150-b, however, decreases by 45%.

The average fabric stress (σ) of SL100-b specimens is 575.4 MPa (see Table 2), which is very close to the stress corresponding to first mortar cracking in tensile tests (567.5 MPa). This observation shows that before the formation of any cracks in the mortar, complete debonding occurs in those samples leading to a substantial decrease in the bond strength of the whole system. On the other hand, the average value of σ in SL150-b specimens is 827.8 MPa, almost equal to the glass yarn strength (875 MPa). This high level of utilization of the strengthening system is due to the combined effect of embedded length and surface preparation. Comparison of the load-slip curves obtained from the pull-out and single-lap tests, see Fig. 6b, shows that a higher peak load and initial stiffness are obtained from the pull-out tests performed on samples with similar embedded lengths (e.g., 100 mm bond length, see Table 2). This difference shows that even when the TRM-to-substrate bond has high quality, there can be a significant difference between the pull-out and single-lap results due to differences in the boundary conditions and stress distribution in these two types of specimens.

3.5 Diagonal compression test results

The load-displacement (vertical and horizontal LVDT measurements) response of the unreinforced and strengthen panels are presented in Fig. 7a. The curves are calculated by the average of axial or transversal LVDTs. The effect of strengthening on the strength of the masonry wallets is considerable, see Table 3. The strengthened panels show increases of 3.07 and 3.70 in the peak load in ISa and ISb wallets, respectively, compared to IU specimens. Also, sandblasting of the surface (in ISb) has led to a 19.8 % increment of the shear strength (compared to ISa wallets).

As for the IU panels, the failure is brittle and composed of sliding along the mortar joint and cracking in masonry units with no considerable crack development before failure (see cracking pattern at failure in Fig. 7b). In ISb wallets, two vertical cracks occur initially in the central region of the TRM composite, followed by tensile rupture of the yarns and further development of axial cracks. The distance between the cracks varied from 100 mm to 35 mm, similar to the crack spacing observed in tensile tests. This observation shows a little difference in ISa specimens, in which the TRM composite partially debonded from the masonry substrate before reaching the maximum load.

The shear stress (τ') and strain (γ) in the center of the panel can be calculated according to ASTM- E 519-2 [39]. The shear stress (τ') can be obtained as:

$$\tau' = \frac{P\cos\theta}{A_n} \quad \text{..... (1)}$$

P and θ are the applied load and the angle between the bed joint and the main diagonal of the wallet, respectively. A_n, which is equal to 5400 mm^2, is the net area of the specimen calculated as follows:

$$A_n = \left(\frac{L + H_w}{2}\right) t.n' \quad \text{..... (2)}$$

where L, H_w, and t are the length, the height, and the thickness of the panel, respectively, and are equal to 540 mm, 540 mm, and 100 mm. n' is the percentage of the gross area of the unit that is solid, expressed as a decimal. The shear strain (γ) is calculated as follows:

$$\gamma = \frac{\Delta_v + \Delta_h}{g} \quad \text{..... (3)}$$

Δ_v, Δ_h, and g are the axial shortening, the transversal extension, and the axial gauge length, respectively.

The average shear stress-strain curves of each series, obtained from the above formulations, are plotted in Fig. 7b. In addition, Table 3 reports the maximum shear stress (τ'_{max}) and its corresponding strain (γ_{max}), as well as the pseudo-ductility ratio ($\mu_{diagonal} = \gamma_u / \gamma_y$) and the shear modulus (G) of each specimen, which are the main parameters characterizing the shear behavior of the masonry wallets [17]. In this study, γ_u is the ultimate shear strain corresponding to a 20 % strength drop on the post-peak softening branch of the shear stress-strain curve [15, 17, 43, 44]. Also, γ_y is introduced as the shear strain at 75 % of the maximum shear stress [13, 14, 17, 45]. Since the IU specimens only bear load until the peak point, γ_u is considered equal to γ_{max} to calculate the pseudo-ductility ratio. Furthermore, G is defined as the secant modulus between 5% and 30% of the maximum shear stress [22, 46].

A comparison between the IU and the strengthened wallets (ISa and ISb) illustrates that strengthening with TRM composite leads to a significant increment of all the parameters mentioned above, as shown in Table 3, which is also in line with previous studies [14, 15, 19, 26]. Sandblasting of the masonry surface seems to have a significant effect on controlling the failure mode and, consequently, the mechanical performance of the strengthened wallets. From Table 3,

τ'_{max}, γ_{max}, and μ of the ISb panels are 1.24, 1.22, and 1.26 times higher than for ISa wallets, respectively; however, sandblasting does not seem to have a significant influence on the shear modulus (G). This observation was expected as bond delamination in ISa panels occurred at later stages of the tests in this case.

Casacci et al. [15] also investigated the in-plane behavior of unreinforced and strengthened masonry panels using a similar TRM system as strengthening material. The panels were tested at 60 days age, and the curing condition of TRM composite was 30 days in the laboratory environmental condition. The maximum shear strength of IU and reinforced wallets (strengthened at both sides) were 0.18 MPa and 0.87 MPa, respectively, while these values for IU and ISa panels tested in the present study are significantly higher (0.6 MPa and 1.78 MPa, respectively). These differences seem to highlight the significant and simultaneous effects of age and curing conditions on the in-plane behavior of panels constructed and strengthened using lime-based mortars.

3.6 Out-of-plane test results

Fig. 8 shows the load-displacement curves and failure modes of the panels failure parallel (P) and normal (N) to the bed joint under out-of-plane loading. In both unreinforced wallet types (PU and NU), a sudden and brittle failure of masonry after the peak load was observed. In PU, a single crack across the panel and along the bed joint was formed (Fig. 8a), whereas, in NU wallets, the cracks initiated in the head joint and progressed around the units in alternate courses (Fig. 8b).

The failure mode of strengthened wallets is also sudden and occurs once the load reaches the tensile strength of the textile, but at a much larger displacement and load capacity, as can be seen in Fig. 8a and Fig. 8b. The number of cracks for PS and NS is two and one wide cracks, respectively, formed in the TRM composites at the constant moment region. Like unreinforced wallets, the PS wallets failed at the masonry bed joint (Fig. 8a), while the NS wallets failed through the masonry units (Fig. 8b), meaning that the presence of TRM composite did not influence the failure mode of the masonry. In contrast to diagonal compression wallets, no TRM-to-masonry detachment was observed in any of these wallets (with and without sandblasting). This behavior can be due to the differences in the stress states in the system compared to the in-plane tests. The average distance between cracks is 125 mm and 113 mm for PSa and PSb, respectively, slightly larger than the crack spacing observed in TRM tensile tests. This difference can be due to the difference in the load application and boundary conditions in these two test methods.

Table 4 reports the main results of the out-of-plane behavior of the wallets tested parallel to the bed joint in terms of the cracking load (P_{cr}) and its corresponding deflection (Δ_{cr}), as well as the maximum load (P_{max}) and its corresponding deflection (Δ_{max}). It can be observed that the application of the glass-based TRM system leads to a significant enhancement of the flexural strength of the panels (37 and 41 times for PSa and PSb, respectively). The deformation capacity of the system is also increased significantly. This parameter can be quantified through the definition of a ductility parameter ($\mu_{bending}$) as follows [19, 47]:

$$\mu_{bending} = \frac{1}{2}\left(\frac{E_{max}}{E_{cr}} + 1\right) \quad \text{..... (4)}$$

where E_{max} is the area under the load-displacement curve until the maximum load (P_{max}) and E_{cr} is the area until the cracking load (P_{cr}). It can be observed in Table 4 that the $\mu_{bending}$ of PSb wallets (sandblasted wallets) is 1.3 times higher than the ductility of the PSa wallets (wallets with no surface treatment). The role of TRM composite in improving the bending behavior of wallets is also significant in wallets tested normal to the bed joints, see Table 4. The maximum load is 3.3 and 2.9 times increased in NSa and NSb, respectively, compared with NU wallets. Sandblasting of the bricks does not show a considerable effect on the out-of-plane behavior. The ductility parameter, however, is higher by 14% in NSb in contrast to NSa.

The orthogonal strength ratio (OSR), a parameter about the anisotropy degree of masonry, is equal to the ratio of the gross area modulus of rupture (R) parallel to bed joints (R_P) to that of normal to bed joints (R_N) [18]. According to ASTM E518 [48], R is expressed as follows:

$$OSR = \frac{R_P}{R_N}, R = \frac{\left(P_{max} + 0.75P_s\right)L_s}{b_m t^2} \quad \text{..... (5)}$$

in which P_s and L_s are the specimen weight and outer span length (420 mm). b_m and t are corresponding to the width and thickness of the panel (b_m= 420 for PS panels and 330 mm for NS panels). Since wallets are tested in the vertical position, the effect of self-weight on the flexural tensile strength is considered to be zero (P_s= 0). Table 4 shows that the OSR for URM wallets is equal to 9.5, which indicates the URM wallets have a high anisotropy degree. Nevertheless, for the PSa and PSb wallets, it is found to be 1.24 and 0.97, respectively, showing that the TRM composite has a crucial role in significantly decreasing the anisotropy degree.

4 Analytical modeling

4.1 Crack spacing prediction of TRM composites

The ACK-theory is used here to calculate/predict the saturation crack spacing in the tensile specimens. Based on this model, the saturation crack spacing (X) can be obtained by expressing the force equilibrium along the loading axis of the yarns [49, 50]:

$$X = 1.337 \frac{\upsilon_m r \sigma_{mu}}{\upsilon_f 2\tau_f} \quad \text{..... (6)}$$

υ_f and υ_m are the volumetric fractions of the yarns, and the mortar, respectively. υ_f is calculated as the ratio between the yarn area mesh and the average cross-section of the specimens (υ_f= 0.00335), while υ_m is equal to 1-υ_f. r is the yarn/cord radius equal to 0.5298 mm for glass yarns (assuming a circular section area). τ_f is the frictional shear strength at the yarn interface and the mortar obtained from the pull-out tests as 2.3 MPa (Table 2). Finally, σ_{mu} is the direct tensile strength of the mortar. In the absence of experimental results, this value can be obtained from the compressive, flexural, or splitting strength [51], as calculated and presented in Table 5. It can be observed that the mortar tensile strength values calculated from these formulations are very similar. Having calculated the τ_f and σ_{mu}, Eq. (6) is used to calculate the saturation crack spacing, see Table 5. It can be observed that the crack spacing is predicted to be around 86~92 mm, which represents a 10~15% error with respect to the experimental results.

4.2 Prediction of panels shear strength

Shear strength of IU panels can be computed based on the failure mode [16, 19, 52, 53]: the shear sliding, the shear friction, the diagonal tension, and the toe crushing. Since sliding along the mortar joint was the failure mode of IU panels, their shear strength (V_{ss}) can be calculated as follows:

$$V_{ss} = \frac{\tau_0}{1 - \mu_0 \tan\theta} A_n \quad \text{..... (7)}$$

where τ_0 is shear bond strength obtained from the shear strength of masonry prisms at 28 days (τ_0= 0.26 MPa), and μ_0 is the coefficient of internal shear friction in mortar joint equal to 0.3 reported in other studies [16, 19]. Other parameters (θ and A_n) are defined in section 3.5. Therefore, V_{ss} is equal to 20.06 kN, showing a 51% error to the experimental results. This difference can

result from μ_0 value. Paulay and Priestly [54] proposed that μ can be between 0.3 and 1.2. If μ is equal to 0.66, the V_{ss} will be 41.3 kN equal to the experimental mean value of IU panels.

The nominal shear capacity (V_n) of TRM-strengthened panels, based on ACI 549.4R-13 [55], consists of the shear strength provided by the masonry (V_m) and the TRM composites (V_f), as shown in Online Resource 2:

$$V_n = V_m + V_f \quad \text{..... (8)}$$

Since all strengthened-masonry panels failed under diagonal tension, the masonry shear strength can be calculated as follows:

$$V_m = \frac{\tan\theta + \sqrt{21.16 + \tan^2\theta}}{10.58} f_t' A_n \left(\frac{L}{H_w}\right) \quad \text{..... (9)}$$

where f'_t is the tensile strength of masonry and equal to $0.67\sqrt{f'_m}$, in which f'_m is the compressive strength of masonry (f'_m= 11.1) as reported by [16, 19, 52], and other parameters (θ, A_n, L, and H_w) are defined in section 3.5. Therefore, the masonry shear strength (V_m) is obtained as 65 kN, which is higher than V_{ss}, and the experimental result of IU panels due to considering different failure modes.

The shear capacity provided by the TRM composites (V_f) can be calculated as [55]:

$$V_f = 2nA_f L f_{fv} \quad \text{..... (10)}$$

where n and A_f are the number of fabric layers (n= 1) and area of fabric per unit width in both directions (A_f= 0.07054mm^2/mm). f_{fv} is the tensile strength in the TRM reinforcement, which is equal to:

$$f_{fv} = E_f \varepsilon_{fv}, \varepsilon_{fv} = \varepsilon_{fu} \le 0.004 \quad \text{..... (11)}$$

where E_f and ε_{fv} are the tensile modulus of elasticity of cracked TRM and the design tensile strain of TRM composites, respectively [55]. Based on ACI 549.4R-13 [55], ε_{fv} should be equal to the ultimate tensile strain of TRM composites (ε_{fu}= ε_3= 0.0119 from Table 2) and less than 0.004, as presented in Eq. (11). It seems this limitation is because of avoiding large cracks in the TRM composites [56]. By examining the tensile behavior of TRM composite in this study (see Fig. 5 and Table 2), it can be seen that ε_{fv} equal to 0.004 occurs precisely at the crack development stage. Having E_f= 62700 MPa from the average of the experimental tensile tests (see Table 2) and ε_{fv}= 0.004, f_{fv} can be obtained as 250.8 MPa. Replacing this value in Eq. (10) will lead to a V_f value of 19 kN. Adding Eq. (9) to Eq. (10) will lead to a total shear capacity of the strengthened

panels of 84 kN, which is 33% and 44% lower than the experimental results of ISa and ISb panels, respectively (Table 6). This observation is also in agreement with the findings of other studies [16, 19, 56]. One possible reason for such a difference between the analytical and experimental results is the erroneous estimation of ε_{fv} in Eq. (11) and the fact that it is limited to 0.004. If ε_{fv} is considered equal to 0.0119, V_f and V_n will be equal to 56.8 kN and 121.8 kN, respectively, which shows a 3% and 19% error to the experimental results ISa and ISb panels, respectively.

Another method to determine f_{fv} is combining the results of TRM-to-substrate bond and direct tensile tests performed on the yarn [57]. Such a combination, presented in Fig. 9, allows the calculation of the effective tensile capacity of the textile under more realistic boundary conditions. Here, the average pull-out load-slip curves obtained from samples with 50 mm and 100 mm bond length are also presented and used to calculate this load (values are presented in Table 6). These three values are then used for predicting the TRM shear contribution (V_f) to obtain the total shear capacity, as presented in Table 6. In this method, the error in the prediction of V_n is less (1~21% for ISa panels and 17~34% for the ISb panels, in general). A comparison between the V_f obtained from the single-lap, and pull-out test results show that although SL100-b specimens have a longer bond length than the pull-out specimens with 50 mm embedded length, they are similar tensile capacity and, consequently, V_f can be obtained from them. Also, the pull-out specimens with 100 mm embedded length show a higher utilization of tensile capacity than the single-lap samples with the same embedded length because of the difference in the boundary conditions in these two test setups. Overall, it appears that the single-lap test results are more suitable for calculating the tensile capacity of TRM systems due to the more realistic boundary conditions imposed on the samples in this test setup. However, it should also be noted that single-lap shear bond tests represent a specific case where the crack surface is perpendicular to the fabric direction. In reality, the cracks occur at an angle to the fabrics, leading to the involvement of transverse fabric in bidirectional grids. These, which can affect the utilized tensile capacity of the fabrics, are not considered when single-lap shear bond tests are used to calculate f_{fv}.

4.3 Prediction of panels flexural strength

The nominal flexural strength of unreinforced masonry panels can be calculated as follows [46]:

$$M_{Rd} = S f_{xk} \quad \text{..... (12)}$$

where S is the section modulus of un-crack wallets (7×10^5 mm^3 and 5.5×10^5 mm^3 for PU and NU panels, respectively). f_{xk} is the flexural strength of masonry and can be calculated based on the masonry unit type and the joint mortar compressive strength [46]. Since the flexural strength of masonry did not measure in this study, f_{xk} is used from what was proposed by EN 1996-1-1 [46]. Hence, f_{xk} is equal to 0.1 MPa and 0.4 MPa for PU and NU panels, respectively. Replacing S and f_{xk} in Eq. (12), M_{Rd} can be obtained for PU and NU panels as 0.07 kN.m and 0.22 kN.m, respectively, showing a 22% and 69% error, in contrast to the experimental results. This difference can be due to the estimated flexural strength of masonry (f_{xk}).

As for the TRM-strengthened masonry, the nominal flexural strength (M_n) can be calculated following ACI 549.4R-13 [55] formulations:

$$M_n = A_f b_m f_{fe}\left(t + \frac{t_c}{2} - \frac{\beta_1 c}{2}\right) \quad \text{..... (13)}$$
$$f_{fe} = E_f \varepsilon_{fe},\ \varepsilon_{fe} = 0.7\varepsilon_{fu} \le 0.012$$

where A_f is the fabric area per unit width (A_f= 0.03572 mm^2/mm), and f_{fe} is the effective tensile stress level in the TRM composite. Also, t and t_c, equal to 100 mm and 10 mm, are masonry wallet and TRM composite thickness. c is the depth of the effective compressive block (see Online Resource 3), and β_1 is a stress block coefficient equal to 0.7. ε_{fe} is the effective tensile strain level in the TRM, and ε_{fu} is the ultimate tensile strain of TRM composites (Table 2). It should be mention since the masonry compressive strength (f'_m) only was measured perpendicular to the flatwise surface of the brick, f'_m is considered the same value for both PS and NS panels. In Eq. (13), it is assumed that plane sections remain plane after loading, TRM has a linear behavior to failure neglecting its contribution before cracking, and the masonry tensile strength is neglected. Online Resource 3 presents the analytical predictions under both failure directions. M_n is equal to 0.80 kN.m and 0.63 kN.m for PS and NS, respectively, lower than the experimental results. Table 6 shows the proportion of M_n to the maximum flexural strength of PS and NS experiments representing a 65~72% error. This observation is also in agreement with the findings of other studies [16, 19, 58].

Based on the approach presented in section 4.2 (the combination of the bond response and the yarn tensile behavior), the effective tensile stress (f_{fe}) level in the TRM composite and the nominal flexural strength (M_n) of PS and NS are presented in Table 6. Combining the pull-out response with 50 mm embedded length and the yarn tensile behavior shows a 70~75% error to the

experimental results (see Table 6). The error resulted from the single-lap shear test (SL100-b), and the pull-out response in 100 mm bond length is 67~74% and 47~57%, respectively. It is obvious that all these methods produce a significant error in the prediction of the flexural capacity of TRM-strengthened masonry.

5 Conclusions

A series of multi-level experimental tests were performed to investigate the effect of glass-based TRM composite and the brick surface treatment on the masonry wallets' behavior. The following main conclusions can be drawn from the experimental results:

- Comparison of the pull-out and debonding (single-lap) shear tests indicated a significant difference in the obtained load-slip curves and failure modes. This difference, being significant even when the TRM-to-substrate bond is of high quality (when the surface is treated) due to the differences in the boundary conditions and stress distribution in these two test methods. While pull-out tests provide information for characterization of the fabric-to-mortar bond behavior, debonding tests provide information on the reliability of the strengthening system used.
- Tensile test results showed that curing conditions significantly affected the tensile response in both uncracked and cracked stages, including the cracking strength and saturated crack spacing. As the curing degree of the mortar increases, both cracking strength and saturated crack spacing increase. While the former is favorable, the latter is unfavorable in structural safety.
- The effect of surface preparation on the TRM-to-substrate bond behavior was significant. The sandblasted specimens showed a perfect bond at the TRM-masonry interface, while delamination was observed in the samples prepared with no surface treatment. In both cases, this had a significant influence on the in-plane response of TRM-strengthened panels. However, this influence was less important in out-of-plane tests because of the tension-compression stresses introduced in the TRM system under the test setup boundary conditions.
- Application of one layer of glass-based TRM, used in this study, was observed to significantly influence the in-plane and out-of-plane response of masonry panels. Both the load and deformation capacity increased significantly. The failure mode of the wallets also

changed from brittle in URM walls to pseudo ductile (limited crack development stage followed by brittle failure) in TRM-strengthened masonry.

- Comparing the experimental results obtained in this study with the ones available in the literature that were performed on similar materials showed the significant and simultaneous effect of age and curing conditions on the structural response of strengthened panels. This significant influence is expected to be dependent on the type of mortar used.
- The crack spacing diagonal compression samples were similar to the saturated crack spacing observed in tensile tests. However, the out-of-plane test samples showed a larger crack spacing due to the differences in these samples' stress conditions, which affects the bond behavior as the main controlling mechanism for mortar crack spacing.
- When combined with pull-out tests results, the ACK theory provided satisfactory predictions of the crack spacing in tensile test samples.
- Analytical prediction of the capacity of strengthened panels required calculation of the textile contribution in the load resistance of the whole system. The existing formulations use the tensile capacity of the textile as an input. Single-lap test results seem to be suitable for calculating the effective tensile capacity of TRM systems. However, it should also be noted that single-lap shear bond tests represent a specific case where the crack surface is perpendicular to the fabric direction. In reality, the cracks occur at an angle with respect to the fabrics which can also lead to involvement of transverse fabric in bidirectional grids. These, which can affect the utilized tensile capacity of the fabrics, are not taken into account and require further investigation.

6 Compliance with ethical standards

This work was partly financed by FCT/MCTES through national funds (PIDDAC) under the R&D Unit Institute for Sustainability and Innovation in Structural Engineering (ISISE), under reference UIDB/04029/2020. The support to the first author through grant agreement SFRH/BD/131282/2017, provided by FCT- Foundation for Science and Technology, is kindly acknowledged.

Conflict of interest: The authors declare that they have no conflict of interest.

7 References

1. Valvona F, Toti J, Gattulli V, Potenza F (2017) Effective seismic strengthening and monitoring of a masonry vault by using Glass Fiber Reinforced Cementitious Matrix with embedded Fiber Bragg Grating sensors. Compos Part B Eng 113:355–370. https://doi.org/10.1016/j.compositesb.2017.01.024
2. Karimi AH, Karimi MS, Kheyroddin A, Shahkarami AA (2016) Experimental and numerical study on seismic behavior of an infilled masonry wall compared to an arched masonry wall. Structures 8:144–153. https://doi.org/10.1016/j.istruc.2016.09.012
3. Marques R, Lourenço PB (2019) Structural behaviour and design rules of confined masonry walls: Review and proposals. Constr Build Mater 217:137–155. https://doi.org/10.1016/j.conbuildmat.2019.04.266
4. Raoof SM, Koutas LN, Bournas DA (2017) Textile-reinforced mortar (TRM) versus fibre-reinforced polymers (FRP) in flexural strengthening of RC beams. Constr Build Mater 151:279–291. https://doi.org/10.1016/j.conbuildmat.2017.05.023
5. Trapko T (2013) The effect of high temperature on the performance of CFRP and FRCM confined concrete elements. Compos Part B Eng 54:138–145. https://doi.org/10.1016/j.compositesb.2013.05.016
6. Padalu PKVR, Singh Y, Das S (2020) Cyclic two-way out-of-plane testing of unreinforced masonry walls retrofitted using composite materials. Constr Build Mater 238:117784. https://doi.org/10.1016/j.conbuildmat.2019.117784
7. De Santis S, de Felice G, Roscini F (2019) Retrofitting of masonry vaults by basalt textile-reinforced mortar overlays. Int J Archit Herit 13:1061–1077. https://doi.org/10.1080/15583058.2019.1597947
8. Valluzzi MR, Modena, Claudio V, de Felice G (2014) Current practice and open issues in strengthening historical buildings with composites. Mater Struct 47:1971–1985. https://doi.org/10.1617/s11527-014-0359-7
9. D'Antino T, Papanicolaou C (2017) Mechanical characterization of textile reinforced inorganic-matrix composites. Compos Part B Eng 127:. https://doi.org/10.1016/j.compositesb.2017.02.034
10. Younis A, Ebead U (2018) Bond characteristics of different FRCM systems. Constr Build Mater 175:610–620. https://doi.org/10.1016/j.conbuildmat.2018.04.216
11. Ferretti F, Mazzotti C (2021) FRCM/SRG strengthened masonry in diagonal compression: experimental results and analytical approach proposal. Constr Build Mater 283:122766. https://doi.org/10.1016/j.conbuildmat.2021.122766
12. Papanicolaou C, Triantafillou T, Lekka M (2011) Externally bonded grids as strengthening and seismic retrofitting materials of masonry panels. Constr Build Mater 25:504–514. https://doi.org/10.1016/j.conbuildmat.2010.07.018
13. Marcari G, Basili M, Vestroni F (2017) Experimental investigation of tuff masonry panels reinforced with surface bonded basalt textile-reinforced mortar. Compos Part B Eng 108:131–142. https://doi.org/10.1016/j.compositesb.2016.09.094
14. Parisi F, Iovinella I, Balsamo A, et al (2013) In-plane behaviour of tuff masonry strengthened with inorganic matrix-grid composites. Compos Part B Eng 45:. https://doi.org/10.1016/j.compositesb.2012.09.068
15. Casacci S, Gentilini C, Di Tommaso A, Oliveira D V. (2019) Shear strengthening of masonry wallettes resorting to structural repointing and FRCM composites. Constr Build

Mater 206:19–34. https://doi.org/10.1016/j.conbuildmat.2019.02.044
16. Babaeidarabad S, Arboleda D, Loreto G, Nanni A (2014) Shear strengthening of un-reinforced concrete masonry walls with fabric-reinforced-cementitious-matrix. Constr Build Mater 65:243–253. https://doi.org/10.1016/j.conbuildmat.2014.04.116
17. Wang X, Lam CC, Iu VP (2018) Experimental investigation of in-plane shear behaviour of grey clay brick masonry panels strengthened with SRG. Eng Struct 162:84–96. https://doi.org/10.1016/j.engstruct.2018.02.027
18. Padalu PKVR, Singh Y, Das S (2018) Efficacy of basalt fibre reinforced cement mortar composite for out-of-plane strengthening of unreinforced masonry. Constr Build Mater 191:1172–1190. https://doi.org/10.1016/j.conbuildmat.2018.10.077
19. Sagar SL, Singhal V, Rai DC, Gudur P (2017) Diagonal Shear and Out-of-Plane Flexural Strength of Fabric-Reinforced Cementitious Matrix–Strengthened Masonry Walletes. J Compos Constr 21:. https://doi.org/10.1061/(ASCE)CC.1943-5614.0000796
20. Martins A, Vasconcelos G, Fangueiro R, Cunha F (2015) Experimental assessment of an innovative strengthening material for brick masonry infills. Compos Part B 80:328–342. https://doi.org/10.1016/j.compositesb.2015.06.012
21. Ferrara G, Caggegi C, Martinelli E, Gabor A (2020) Shear capacity of masonry walls externally strengthened using Flax-TRM composite systems : experimental tests and comparative assessment. Constr Build Mater 261:. https://doi.org/10.1016/j.conbuildmat.2020.120490
22. Wang X, Lam CC, Iu VP (2019) Comparison of different types of TRM composites for strengthening masonry panels. Constr Build Mater 219:184–194. https://doi.org/10.1016/j.conbuildmat.2019.05.179
23. Harajli M, Elkhatib H, San-jose JT (2010) Static and cyclic out-of-plane response of masonry walls strengthened using textile-mortar system. J Mater Civ Eng 22:1171–1181. https://doi.org/10.1061/(ASCE)MT.1943-5533.0000128
24. Kariou FA, Triantafyllou SP, Bournas DA, Koutas LN (2018) Out-of-plane response of masonry walls strengthened using textile-mortar system. Constr Build Mater 165:769–781. https://doi.org/10.1016/j.conbuildmat.2018.01.026
25. Basili M, Vestroni F, Marcari G (2019) Brick masonry panels strengthened with textile reinforced mortar: experimentation and numerical analysis. Constr Build Mater 227:117061. https://doi.org/10.1016/j.conbuildmat.2019.117061
26. Shabdin M, Zargaran M, Attari NKA (2018) Experimental diagonal tension (shear) test of Un-Reinforced Masonry (URM) walls strengthened with textile reinforced mortar (TRM). Constr Build Mater 164:704–715. https://doi.org/10.1016/j.conbuildmat.2017.12.234
27. (2005) ASTM C109/C109M-05, Standard test method for compressive strength of hydraulic cement mortars (Using 2-in. or [50-mm] Cube Specimens)
28. (1999) BS EN 1015-11, Methods of test for mortar for masonry. Determination of flexural and compressive strength of hardened mortar
29. (2013) BS EN 12390-13, Testing hardened concrete. Determination of secant modulus of elasticity in compression
30. (2004) ASTM C496/C496M- 04, Standard test method for splitting tensile strength of cylindrical concrete specimens
31. (2005) ASTM C67-05, Standard test methods for smpling and testing brick and structural clay tile
32. (2000) EN 772-1. Methods of test for masonry units – Part 1: Determination of compressive

strength
33. (2003) ASTM C1314-03, Standard test method for compressive strength of masonry prisms
34. (2002) BS EN 1052-3, Methods of test for masonry- Part 3: Determination of initial shear strength
35. Dalalbashi A, Ghiassi B, Oliveira DV, Freitas A (2018) Effect of test setup on the fiber-to-mortar pull-out response in TRM composites: experimental and analytical modeling. Compos Part B Eng 143:250–268. https://doi.org/10.1016/j.compositesb.2018.02.010
36. Dalalbashi A, Ghiassi B, Oliveira D V. (2019) Textile-to-mortar bond behaviour in lime-based textile reinforced mortars. Constr Build Mater 227:116682. https://doi.org/10.1016/j.conbuildmat.2019.116682
37. Razavizadeh A, Ghiassi B, Oliveira D V. (2014) Bond behavior of SRG-strengthened masonry units: Testing and numerical modeling. Constr Build Mater 64:387–397. https://doi.org/10.1016/j.conbuildmat.2014.04.070
38. Ghiassi B, Oliveira D V, Marques V, et al (2016) Multi-level characterization of steel reinforced mortars for strengthening of masonry structures. Mater Des 110:903–913. https://doi.org/10.1016/j.matdes.2016.08.034
39. (2002) ASTM E519-02, Standard test method for diagonal tension (shear) in masonry assemblages
40. (1999) BS EN 1052-2, Methods of test for masonry- Part2: Determination of flexural strength.
41. Dalalbashi A, Ghiassi B, Oliveira D V. (2021) Aging of lime-based TRM composites under natural environmental conditions. Constr Build Mater 270:. https://doi.org/10.1016/j.conbuildmat.2020.121853
42. Dalalbashi A, Ghiassi B, Oliveira DV, Freitas A (2018) Fiber-to-mortar bond behavior in TRM composites: effect of embedded length and fiber configuration. Compos Part B Eng 152:43–57. https://doi.org/10.1016/j.compositesb.2018.06.014
43. Mahmood H, Ingham JM (2011) Diagonal compression testing of FRP-retrofitted unreinforced clay brick masonry wallettes. J Compos Constr 15:810–820. https://doi.org/10.1061/(ASCE)CC.1943-5614.0000209
44. Gattesco N, Boem I (2015) Experimental and analytical study to evaluate the effectiveness of an in-plane reinforcement for masonry walls using GFRP meshes. Constr Build Mater 88:94–104. https://doi.org/10.1016/j.conbuildmat.2015.04.014
45. Babaeidarabad S, De Caso F, Nanni A (2014) URM walls strengthened with fabric-reinforced cementitious matrix composite subjected to diagonal compression. J Compos Constr 18:1–9. https://doi.org/10.1061/(ASCE)CC.1943-5614.0000441.
46. European Committee for Standardization EN 1996-1-1: 2005, Eurocode 6- Design of masonry structures- Part 1-1: General rules for reinforced and unreinforced masonry structures
47. Galal K, Sasanian N (2010) Out-of-plane flexural performance of GFRP-reinforced masonry walls. J Compos Constr 14:162–174. https://doi.org/10.1061/(ASCE)CC.1943-5614.0000061
48. (2003) ASTM E518-02, Standard test method for flexural bond strength of masonry
49. Aveston J, Cooper G, Kelly A (1971) Single and multiple fracture, the properties of fibre composites. In: Proceedings of the conference national physical laboratories. London: IPC Science and Technology Press Ltd., pp 15–24
50. Cuypers H, Wastiels J (2006) Stochastic matrix-cracking model for textile reinforced

cementitious composites under tensile loading. Mater Struct 39:777–786. https://doi.org/10.1617/s11527-005-9053-0
51. (2011) The fib Model Code for Concrete Structures 2010
52. Li TT., Galati NN., Tumialan JG. G, Nanni A (2005) Analysis of unreinforced masonry concrete walls strengthened with glass fiber-reinforced polymer bars. ACI Struct J 102:569–577
53. ACI Committee 440 (2010) ACI 440.7R-10 Guide for design and construction of externally bonded FRP systems for strengthening unreinforced masonry structures
54. Paulay T, Priestely MJN (1992) Seismic design of reinforced concrete and masonry buildings. Wiley Interscience
55. ACI Committee 549 (2013) ACI 549.4R-13 Design and construction of externally bonded Fabric-Reinforced Cementitious Matrix (FRCM) systems for repair and strengthening concrete and masonry Structures
56. Del Zoppo M, Di Ludovico M, Balsamo A, Prota A (2019) Experimental in-plane shear capacity of clay brick masonry panels strengthened with FRCM and FRM composites. J Compos Constr 23:04019038. https://doi.org/10.1061/(ASCE)CC.1943-5614.0000965
57. CNR DT 215/2018 (2018) Guide for the design and construction of externally bonded fibre reinforced inorganic matrix systems for strengthening existing structures
58. D'Antino T, Carozzi FG, Colombi P, Poggi C (2018) Out-of-plane maximum resisting bending moment of masonry walls strengthened with FRCM composites. Compos Struct 202:881–896. https://doi.org/10.1016/j.compstruct.2018.04.054

8 Supplementary

Online Resource 1. Experimental program.

Objective	Conducted tests	Material	Brick surface	Name
Material characterization test	Compressive test	M1 and M2 mortar, brick	-	-
	Flexural test	M1 and M2 mortar, brick		-
	Elastic modulus test	M1 and M2 mortar, brick		-
	Splitting test	M1 and M2 mortar		-
	Tensile test	glass yarn		-
Textile-to-mortar bond behavior	Single-sided pull-out test	M1 mortar and glass yarn		-
TRM tensile behavior	Tensile test	M1 mortar and glass yarn		-
TRM-to-brick bond behavior	Single-lap shear test	TRM and brick	Original (method a)	SL100-a
			Sandblasted (method b)	SL100-b, SL150-b
In-plane behavior of strengthened masonry	Diagonal compression test	Masonry wallet (URM)	-	IU
		Masonry wallet and TRM	Original (method a)	ISa
			Sandblasted (method b)	ISb
Out-of-plane behavior of strengthened masonry	Bending test, failure parallel and normal to bed joint	Masonry wallet (URM)	-	PU/ NU
		Masonry wallet and TRM	Original (method a)	PSa/ NSa
			Sandblasted (method b)	PSb/ NSb

Online Resource 2. Analytical prediction of shear strength of reinforced panels.

Masonry properties		**Masonry contribution (V_m)**
Height of the wall [mm]	H_w= 540	$V_m = \frac{\tan\theta + \sqrt{21.16 + \tan^2\theta}}{10.58} f_t^{'} A_n \left(\frac{L}{H_w}\right) =$ $\frac{\tan 45 + \sqrt{21.16 + \tan^2 45}}{10.58} 2.23 \times 54000 \left(\frac{540}{540}\right) = 65025\,\text{N}$
Length of the wall [mm]	L= 540	
Net cross-sectional area [mm^2]	A_n= 54000	
Compressive strength of masonry [Mpa]	$f_m^{'} = 11.1$	
Tensile strength of masonry [Mpa]	$f_t^{'} = 0.67\sqrt{f_m^{'}} = 2.23$	
The inclined angle between the horizontal and main diagonal of the wall	θ= 45°	
TRM properties		**TRM contribution (V_f)**
Area of fabric per unit width in both directions [mm^2/mm]	A_f= 2×0.03527= 0.07054	$\varepsilon_{fv} = \varepsilon_{fu} = 0.0119 \not\leq 0.004 \Rightarrow \varepsilon_{fv} = 0.004$ $f_{fv} = E_f \varepsilon_{fv} = 62700 \times 0.004 = 250.8\,\text{MPa}$
Ultimate tensile strain of TRM [mm/mm]	ε_{fu}= 0.0119	$V_f = 2nA_f Lf_{fv} = 2 \times 1 \times 0.07054 \times 540 \times 250.8 = 19106\,\text{N}$
Tensile modulus of elasticity of cracked TRM [MPa]	E_f= 62700	**Nominal shear capacity (V_n)**
Number of fabric layers	n= 1	$V_n = V_m + V_f$= 65025+ 19106= 84131 N= 84 kN

Online Resource 3. Analytical prediction of flexural strength of reinforced panels.

Masonry properties	
Thickness of the masonry wallet [mm]	t= 100
Width of the masonry wallet considered in the flexural analysis [mm]	b_m= 420 and 330 for masonry PS and NS, respectively
Compressive strength of masonry [MPa]	$f'_m = 11.1$
TRM properties	
Area of fabric per unit width [mm^2/mm]	A_f= 0.03527
Effective tensile strain level in the TRM [mm/mm]	$\varepsilon_{fe} = 0.7\varepsilon_{fu} = 0.7 \times 0.0119 = 0.0083 \le 0.012 \Rightarrow \varepsilon_{fe} = 0.0083$
Tensile modulus of elasticity of cracked TRM [MPa]	E_f= 62700
Thickness of TRM composite [mm]	t_c= 10
Flexural strength	
Effective tensile stress level in the TRM composite [MPa]	$f_{fe} = E_f\ \varepsilon_{fe} = 62700 \times 0.0083 = 520.41$
Stress block coefficient related to c	β_1= 0.7
Stress block coefficient related to f'$_m$	γ= 0.7
Depth of effective compressive block [mm]	$c = \frac{A_f f_{fe}}{\gamma f'_m \beta_1} = \frac{0.03527 \times 520.41}{0.7 \times 11.1 \times 0.7} = 3.375$
Nominal flexural strength [N.mm]	$M_n = A_f b_m f_{fe}\left(t + \frac{t_c}{2} - \frac{\beta_1 c}{2}\right) =$
for PS (failure parallel to bed joint):	$0.03527 \times 420 \times 520.41\left(100 + \frac{10}{2} - \frac{0.7 \times 3.375}{2}\right) = 800343$
for NS (failure normal to bed joint):	$0.03527 \times 330 \times 520.41\left(100 + \frac{10}{2} - \frac{0.7 \times 3.375}{2}\right) = 628840$

Table 1. Mechanical properties of the mortars and the brick.*

Strength [MPa]	M1 mortar		M2 mortar		Brick			Number of specimens for each test material type
	28 days	90 days	28 days	120 days	flatwise	lengthwise	widthwise	
Compressive strength	12.0 (5)	16.8 (11)	5.3 (6)	8.7 (6)	23.5 (5)	22.3 (10)	18.6 (10)	5
Flexural strength	4.7 (8)	4.5 (2)	1.7 (9)	1.7 (9)	4.5 (14)	4.4 (4)	-	5
Splitting tensile strength	0.9 (7)	1.4 (8)	0.3 (11)	0.5 (7)	-	-	-	5
Elastic modulus	6993 (11)	6713 (6)	-	5236 (10)	-	-	9650 (2)	5

*CoV of the results is given in percentage inside parentheses.

Table 2. Mechanical properties of TRM composites.*

Test	P_P [N]	S [mm]	$E_{deb.}$ [N.mm]	$E_{pull.}$ [N.mm]	K [N/mm]	τ_{max} [MPa]	τ_f [MPa]	κ [N/mm^3]	β	-	-	Number of specimens
Pull-out (50 mm)	410.3 (12)	0.37 (47)	107.3 (49)	4366.3 (23)	1602.0 (6)	3.2 (13)	2.3 (16)	23.2 (20)	0.0001 (0)	-	-	5
Pull-out (100 mm)	722.5 (7)	1.18 (25)	592.9 (32)	-	2253.3 (37)	-	-	-	-	-	-	5
-	E_1 [GPa]	E_2 [GPa]	E_3 [GPa]	ε_1 [%]	ε_2 [%]	ε_3 [%]	σ_1 [MPa]	σ_2 [MPa]	σ_3 [MPa]	N.C.	D.C. [mm]	-
Tensile	2280.0 (25)	19.4 (28)	62.7 (15)	0.03 (25)	0.68 (30)	1.19 (9)	567.5 (12)	695.0 (5)	995.6 (9)	3 (13)	101 (23)	4
-	P_P [N]	S [mm]	σ [MPa]	K [N/mm]	-	-	-	-	-	-	-	-
SL100-a	237.57 (22)	0.56 (32)	269.43 (22)	461.3 (47)	-	-	-	-	-	-	-	5
SL100-b	507.3 (25)	1.20 (29)	575.4 (25)	975.7 (48)	-	-	-	-	-	-	-	5
SL150-b	729.9 (6)	1.59 (18)	827.8 (6)	445 (28)	-	-	-	-	-	-	-	5

*CoV of the results is given in percentage inside parentheses.
N.C.: Number of cracks, D.C.: Distance between cracks

Table 3. Diagonal compression test results. *

Specimen	P_{max} [kN]	Failure	τ'_{max} [MPa]	γ_{max} [%]	γ_y [%]	γ_u [%]	$\mu_{diagonal}$	G [MPa]	Number of specimens
IU	41.04 (22)	A & B	0.60 (31)	0.07 (47)	0.04 (40)	0.07 (47)	1.97 (13)	1815 (76)	3
ISa	126.04 (6)	D & A	1.78 (6)	0.09 (2)	0.06 (4)	0.16 (35)	2.74 (37)	2402 (8)	3
ISb	151.01 (0)	E & C	2.20 (1)	0.11 (3)	0.07 (2)	0.24 (1)	3.46 (2)	2488 (1)	2

*CoV of the results is given in percentage inside parentheses.
A: combined sliding along mortar joint and cracking in the masonry units; B: sliding along mortar joint; C: cracking in the masonry units; D: TRM failure with debonding between TRM and the masonry; E: TRM failure

Table 4. Flexural test results.*

Specimen	Δ_{cr} [mm]	P_{cr} [kN]	Δ_{max} [mm]	P_{max} [kN]	M_{max} [kN.m]	M_{Rd}/M_{max} [%]	E_{cr} [kN.mm]	E_{max} [kN.mm]	$\mu_{bending}$	R [N/mm^2]	OSR	Number of specimens
PU	-	-	1.05 (37)	1 (34)	0.09 (34)	78	-	1 (50)	-	0.15 (34)	9.50	3
PSa	0.48 (15)	24 (6)	3.02 (21)	37 (19)	2.30 (19)	-	7 (11)	85 (33)	7 (35)	3.67 (19)	1.24	3
PSb	0.36 (1)	22 (10)	2.81 (3)	41 (1)	2.58 (1)	-	5 (11)	82 (9)	9 (2)	4.13 (1)	0.97	3
NU	0.26 (51)	10 (21)	1.95 (51)	11 (33)	0.70 (33)	31	2 (72)	20 (71)	7 (57)	1.42 (33)	-	3
NSa	0.20 (18)	27 (7)	1.76 (4)	36 (13)	2.23 (13)	-	4 (25)	47 (12)	7 (10)	4.55 (13)	-	3
NSb	0.18 (13)	28 (13)	1.83 (8)	32 (23)	1.97 (23)	-	3 (29)	46 (15)	8 (16)	4.01 (23)	-	3

*CoV of the results is given in percentage inside parentheses.

Table 5. Prediction of saturated crack spacing.

Calculating tensile strength by	σ_{mu} [MPa]	$X_{nom.}$ [mm]	$X_{nom.}/X_{exp.}$ [%]
compressive strength (f_{ck})	$0.3\left(f_{ck}\right)^{2/3} = 0.3\left(16.8\right)^{2/3} = 1.97$	91	90
flexural strength ($f_{ctm.fl}$)	$\frac{0.06h_b^{0.7}}{1+0.06h_b^{0.7}} f_{ctm.fl} = \frac{0.06\times 40^{0.7}}{1+0.06\times 40^{0.7}} 4.5 = 1.99$	92	91
splitting strength ($f_{ctm,sp}$)	$2.2\left(f_{cm}\right)^{-0.18} f_{ctm,sp} = 2.2\left(16.8\right)^{-0.18} \times 1.4 = 1.85$	86	85

Table 6. Prediction of the nominal shear capacity (V_n).

Model	f_{fv} [MPa]	V_f [kN]	V_n [kN]	V_n/P_{max} [%]		f_{fe} [MPa]	$M_{n,PS}$ [kN.m]	$M_{n,NS}$ [kN.m]	M_n/M_{max} [%]			
				ISa	ISb				PSa	PSb	NSa	NSb
ACI [55]	250.8	19.1	84.0	67	56	520.4	0.80	0.63	35	31	28	32
Combination of pull-out (50 mm) and tensile behavior	452.5	34.5	99.5	79	66	452.5	0.70	0.55	30	27	25	28
Combination of single-lap (SL100-b) and tensile behavior	486.8	37.1	102.1	81	68	486.8	0.75	0.59	33	29	26	30
Combination of pull-out (100 mm) and tensile behavior	793.3	60.4	125.4	99	83	793.3	1.21	0.95	53	47	43	48

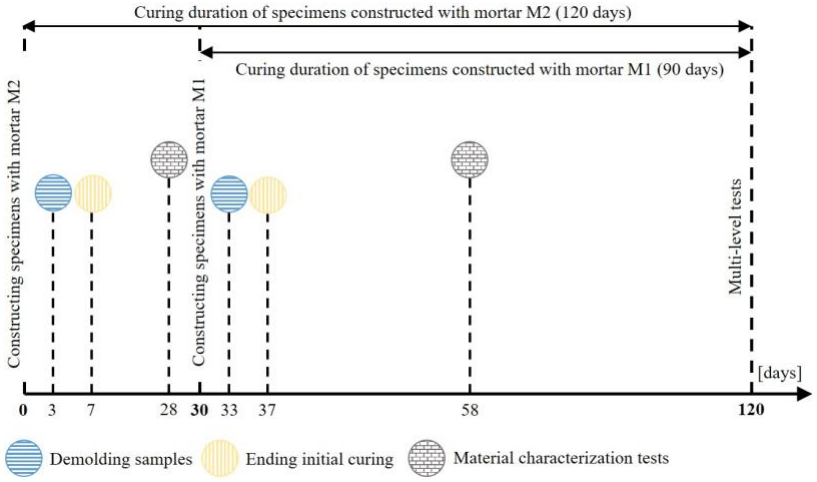

Fig. 1. Schematic representation of the test program.

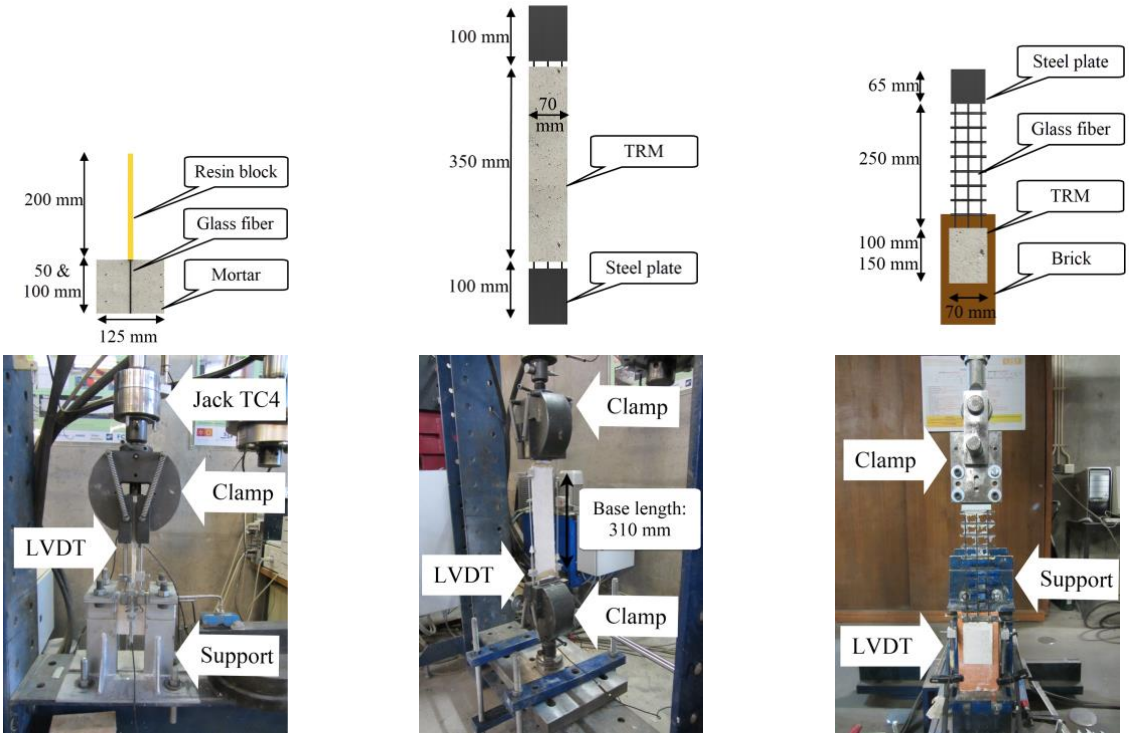

(a) (b) (c)

Fig. 2. Geometrical and test setups details of the samples: (a) pull-out test; (b) tensile test; (c) single-lap shear test.

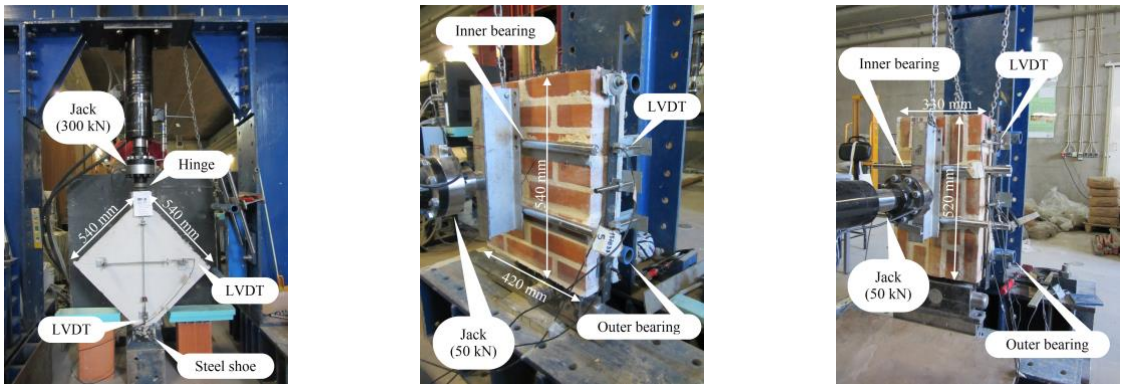

(a) (b) (c)

Fig. 3. Test setups (a) diagonal compression test; (b) bending test, failure parallel to bed joint; (c) bending test, failure normal to bed joints.

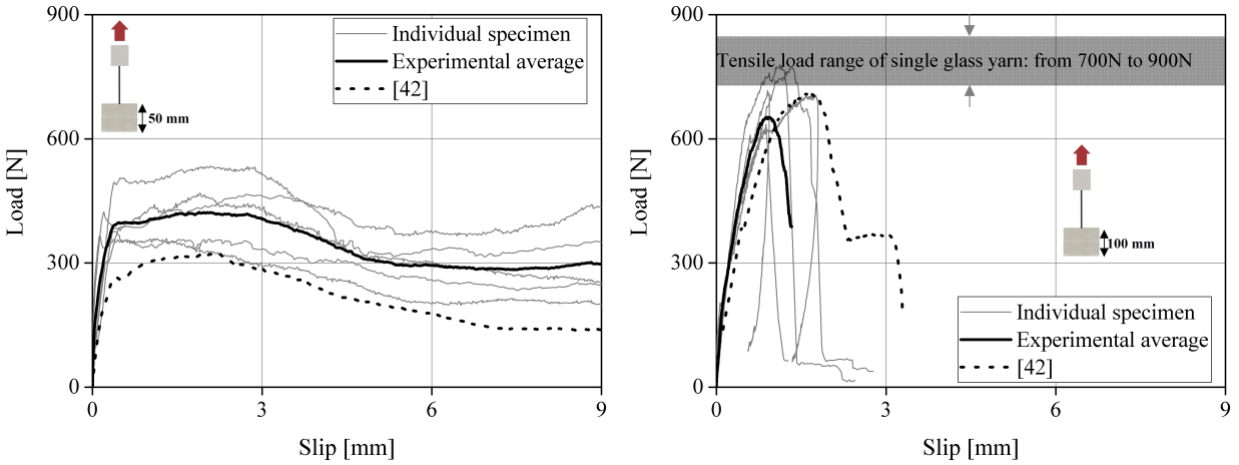

(a) (b)

Fig. 4. Pull-out response of TRM composite: (a) bond length= 50 mm; (b) bond length= 100 mm.

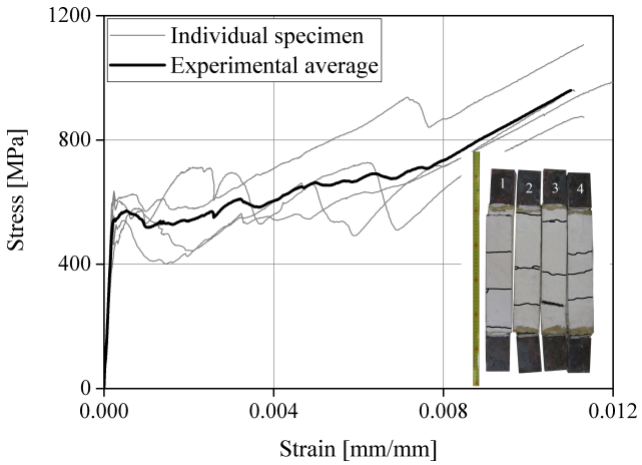

Fig. 5. Tensile behavior of TRM composite.

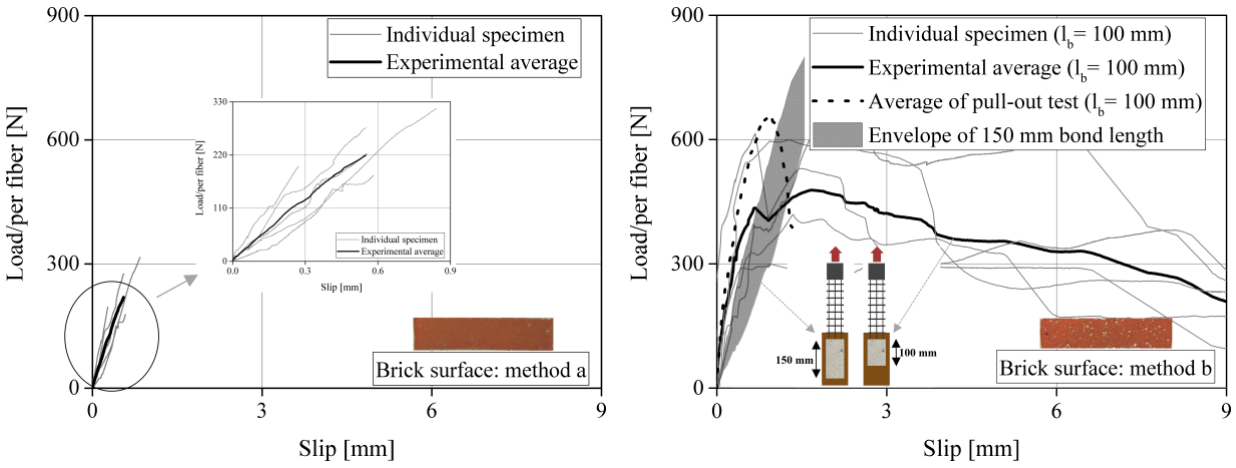

(a) (b)

Fig. 6. TRM-to-substrate bond behavior: (a) original brick; (b) sandblasted brick.

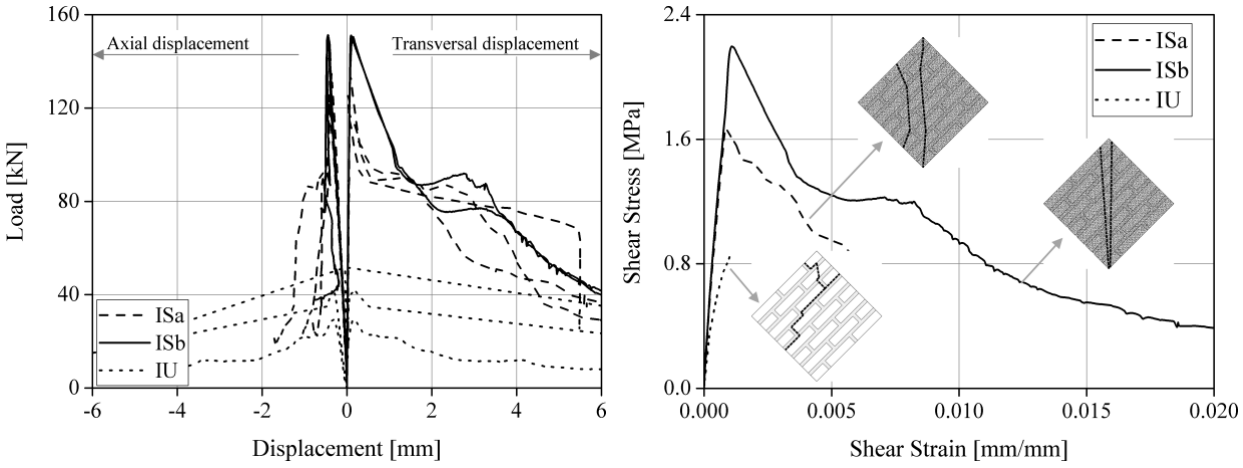

(a) (b)

Fig. 7. Diagonal compression result: (a) load-displacement curves; (b) average shear stress-strain curves.

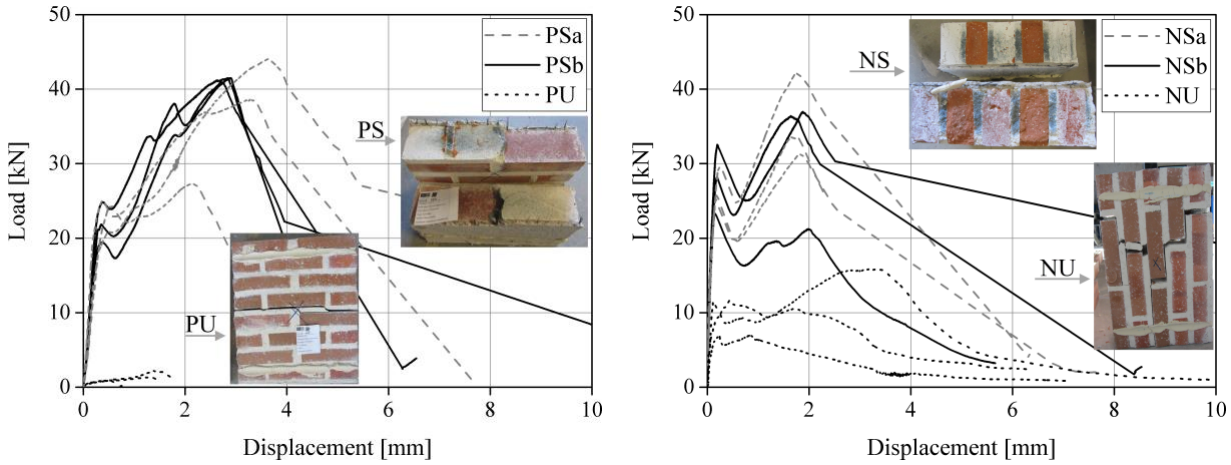

Fig. 8. Load-displacement curves of flexural tests: (a) failure parallel to bed joint; (b) failure normal to bed joint.

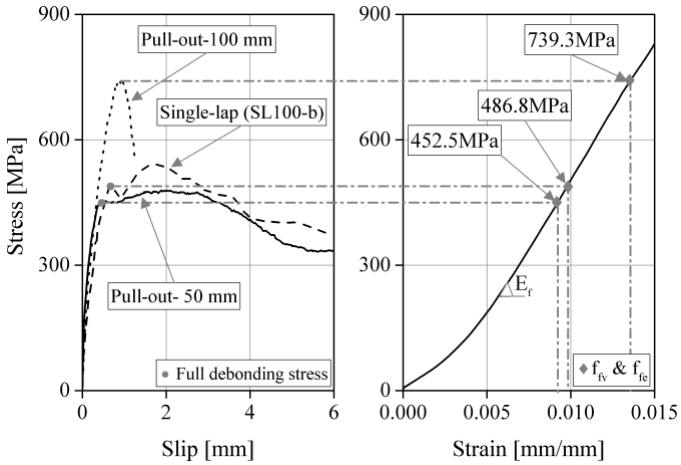

Fig. 9. Interaction between bond responses and tensile stress-strain of the yarn.